Dalton Transactions

ROYAL SOCIETY OF CHEMISTRY

PAPER

View Article Online
View Journal | View Issue

Cite this: *Dalton Trans.*, 2023, **52**, 7701

Oxidation-induced C–H bond activation in iridium pincer complexes†

Alexey V. Polukeev * and Magdalena Tasić

Dehydrogenation reactions that produce molecular hydrogen are thermodynamically unfavourable. Desired is to couple them with a green driving force, such as oxidation with oxygen or an electric current. This, in turn, requires understanding of the catalyst's redox properties. Here we report oxidation of the iridium pincer complexes (POCOP)IrHCl (POCOP = 2,6-(^{t}Bu$_2$PO)$_2$C$_6$H$_3$; **1a**) and (PCP)IrHCl (PCP = 2,6-(^{t}Bu$_2$PCH$_2$)$_2$C$_6$H$_3$; **1c**) that induced intramolecular C–H activation, followed by the formation of complexes with a cyclometallated *tert*-butyl group. Based on an electrochemical study and DFT calculations, we propose a mechanism that involves H$^+$ loss from hydrochlorides **1a** and **1c** to give a highly reactive (pincer)IrCl$^+$ compound.

Received 24th March 2023,
Accepted 8th May 2023

DOI: 10.1039/d3dt00903c

rsc.li/dalton

Introduction

Enabling the selective, large-scale functionalization of C–H bonds has long been a tantalizing goal since it may allow for the efficient conversion of the most abundantly available carbon-based feedstocks, alkanes, into more valuable commodity chemicals and raw materials for the chemical industry.[1] Much of the progress in the area is associated with iridium pincer complexes,[2,3] the most efficient catalysts for alkane dehydrogenation, a reaction that converts alkanes into much more reactive olefins. One of the fundamental problems of homogeneous alkane dehydrogenation is the endothermicity of the reaction, which typically requires the presence of a sacrificial hydrogen acceptor. The same often applies to related cross-dehydrogenative coupling reactions.[4] To avoid the use of a sacrificial hydrogen acceptor, attempts were made to couple dehydrogenation with secondary reactions.[1,3] In this respect, there is a growing interest in using oxidation, especially with molecular oxygen, as a driving force for dehydrogenation or C–H activation in general.[5] Attractive is also to use electric current as an oxidant,[6] thus performing a sort of catalytic electrolysis of alkanes.

While there are some successes in iridium promoted C–H bond oxidations,[7] primarily utilizing a Cp*Ir fragment, redox properties and reactions of iridium pincer-ligated complexes only recently attracted the attention of researchers. Thus, it was shown that (Phebox)Ir(OAc)$_2$(H$_2$O) (Phebox = bis(oxazolinyl)phenyl$^-$ NCN pincer ligand) can stoichiometrically activate C–H bonds[8,9] *via* a concerted metallation deprotonation pathway;[10] after reaction, this complex can be regenerated by O$_2$.[11] Conditions required for these two processes are dramatically different though, which precludes the organization of a catalytic cycle.[11] With a milder oxidant, Ag$_2$O, some conversion of mesitylene to 3,5-dimethylbenzaldehyde and 3,5-dimethylbenzoic acid by (Phebox)Ir(OAc)$_2$(H$_2$O) and (Phebox)Ir(OCOCF$_3$)$_2$(H$_2$O) was achieved.[12] Electrochemical and chemical hydride loss from (PCP)IrH$_2$ (PCP = 2,6-(CH$_2$P^{t}Bu$_2$)$_2$C$_6$H$_3$) were investigated;[13] more recently, it was shown[14,15] that, through the addition of a base, such hydride loss can generate active 14e (pincer)Ir species that are known to react with C–H bonds.[3]

Previously, we reported the reaction of (*p*-X–POCOP)IrHCl complexes **1a** and **1b** with several protic acids to give compounds with cyclometallated *tert*-butyl group (Scheme 1).[16] The cleanest transformation was observed with CF$_3$COOH. Some mechanistic studies performed[17] suggested two possible mechanisms: (a) protonation of the hydride ligand and (b) redox processes at the iridium centre.

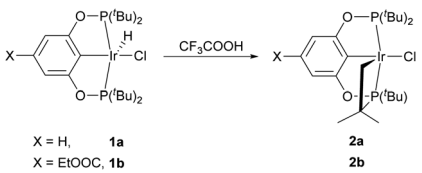

Scheme 1 Reactions of (*p*-X–POCOP)IrHCl iridium pincer complexes with CF$_3$COOH.

Centre for Analysis and Synthesis, Department of Chemistry, Lund University, P.O. Box 124, SE-221 00 Lund, Sweden. E-mail: alexey.polukeev@chem.lu.se

†Electronic supplementary information (ESI) available: Additional electrochemical data, table of coordinates for compounds used in DFT calculations. CCDC 2251444. For ESI and crystallographic data in CIF or other electronic format see DOI: https://doi.org/10.1039/d3dt00903c

Results and discussion

Oxidation-induced cyclometallation

To get more insight into the latter opportunity, we investigated the reaction of complex **1a** with a mild chemical oxidant, CF_3COOAg. It was found that addition of one equivalent of CF_3COOAg to **1a** in THF (or DCM) led to an anion exchange and the formation of trifluoroacetate complex **1a-COOCF$_3$** within seconds, while the addition of excess CF_3COOAg resulted in the formation of metallic silver, cyclometallation of the *tert*-butyl group and the formation of compound **2a-COOCF$_3$** within 30 min in a 90% isolated yield (Scheme 2).

The trifluoroacetate complex **1a-COOCF$_3$** is characterized by resonances at 172.0 (s) and −38.98 (t, $^3J_{PH}$ = 12.7 Hz) ppm in the $^{31}P\{^1H\}$ and ^1H NMR spectra, correspondingly, with other signals being quite featureless. For complex **2a-COOCF$_3$**, an AX system (159.1 and 113.5 ppm, d, $^2J_{PP}$ = 367.4 Hz) in the $^{31}P\{^1H\}$ NMR spectrum, as well as doublets from the CH_3 groups at 1.42 ($^3J_{PH} \approx$ 15.7 Hz) and 0.95 ppm ($^3J_{PH}$ = 12.4 Hz) and multiples from the –CH_2– group at 2.79 and 2.06 ppm indicate metallation of one of the *tert*-butyl groups. In the $^{13}C\{^1H\}$ NMR spectrum, a signal at −3.90 ppm (dd, $^2J_{CP1}$ = 25.4 Hz, $^2J_{CP2}$ = 2.3 Hz) is observed, corresponding to the cyclometallated aliphatic carbon. These features closely resemble spectra of the related phosphinite complexes **2a** and **2b**.[16]

When DDQ and Me_3NO were tried as alternative oxidants, mainly decomposition of **1a** and dismantling of the pincer ligand were observed. However, the formation of **2a** was detected when acetyl–ferrocenium hexafluorophosphate [FcAc]PF_6 was used.

We have also attempted the oxidation of complex (PCP)IrHCl (**1c**), which is a counterpart of **1a** with –CH_2– groups instead of –O– in the pincer arms. The reaction with CF_3COOAg was much less clean than that with **1a**, but the use of [FcAc]PF_6 provided the respective product with a cyclometallated *tert*-butyl, **2c** (Scheme 3).

Other relevant observations include an attempt to oxidize the ruthenocene-based heterobimetallic[18] complex $^{[Ru]}$(PCP)IrHCl (**3**) with CF_3COOAg that led to the observation of AX-systems in the $^{31}P\{^1H\}$ NMR and a disappearance of the hydride resonance, that we interpret as the formation of structures with *exo* and *endo* cyclometallated *tert*-butyl groups (see ESI† for details), and the oxidation of the (PCP)IrHI (**1c-I**) complex with atmospheric oxygen in a C_6D_6 solution that provided **2c-I**. Due to the instability and small amounts of available material these two examples received only a limited characterization *in situ*. They prove, however, that the oxidation-induced C–H bond activation may not be an uncommon reactivity pattern. Also, metallation of a *tert*-butyl group upon deprotection of **1d** (X = O-TBDMS) under oxidative conditions was reported.[19]

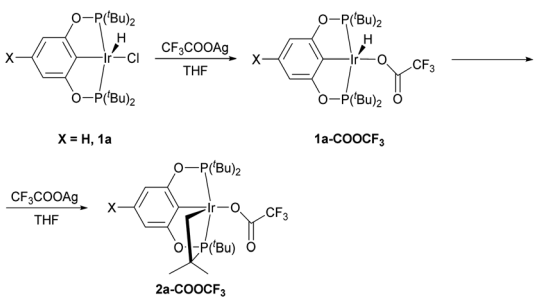

Scheme 2 Reaction of complex **1a** with CF_3COOAg.

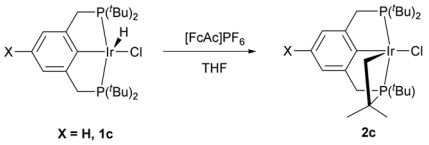

Scheme 3 Reaction of complex **1c** with [FcAc]PF_6.

A(na)gostic bonding in 2a-COOCF$_3$ and related complexes

An XRD structure of complex **2a-COOCF$_3$** is depicted in Fig. 1. Trifluoroacetate is coordinated in a monodentate mode. One of the *tert*-butyl C–H bonds is clearly directed towards the site *trans* to the four-membered metallacycle. Judging from the C–Ir = 3.16 Å and H–Ir ≈ 2.5 Å distances, this site is occupied by an agostic (3c–2e interaction) or an anagostic[20,21] ($Ir^{\delta-}\cdots H^{\delta+}$ interaction) Ir···H–C bond. This type of bonding was not found in the electronically very similar parent hydrido-trifluoroacetate **1a-COOCF$_3$** or hydrido-chlorides **1a** and **1c** neither experimentally nor computationally, and thus is possibly a result of the four-membered metallacycle constraining the *tert*-butyl in a favourable conformation. It is believed that

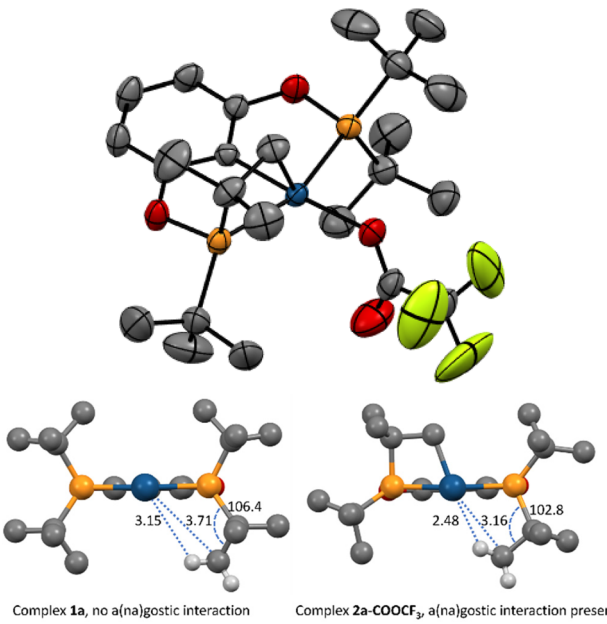

Fig. 1 Top: ORTEP plot of complex **2a-COOCF$_3$**. Ellipsoids are given at a 50% probability level. Hydrogen atoms are omitted for clarity. Bottom: a schematic comparison of XRD structures of **1a**[23] and **2a-COOCF$_3$**. Hydrogen atoms (except for one methyl group) as well as –Cl and –$COOCF_3$ ligands are omitted for clarity.

agostic bonds are characterized by an up-field shift of the bound hydrogen *versus* the non-coordinated one in the ^{1}H NMR spectra, while for anagostic bonds a downfield shift should be observed.[20] Even though such shifts would be averaged over the *tert*-butyl group, we were expecting them to be revealed in a series of related compounds **2a-COOCF$_3$**, **2a**, **2c**, and the *p*-MeO-substituted counterpart of **2c**, (*p*-MeO-PCP) IrHCl (**2e**).[22] However, in the experimental NMR spectra of those compounds little, if any, changes associated with the presence of a(na)gostic bonds were isolated. DFT calculations were then performed that provided some rationale. The selected data for a series of compounds studied is given in Table 1. The Ir···H–C bonding is well captured in the calculated structures. If the chemical shift is taken as a criterion, the bond should be classified as agostic, despite the comparatively long Ir···H distances.

For complex **2a-COOCF$_3$** with the weakest agostic bond, the calculated δ(Ir···H–C) in ^{1}H NMR (0.75 ppm) in fact falls in the range observed for other *tert*-butyl type hydrogens (0.56–1.86 ppm). Presumably, this is because the bound hydrogen, in addition to the agostic bond that is expected to feature an up-field shift, is involved in a hydrogen bond with the oxygen from the –COOCF$_3$ group (H···O = 2.39 Å), that is expected to feature a counter-balancing down-field shift. For complexes **2a**, **2c** and **2e**, the agostic bond becomes stronger, and δ(Ir···H–C) appears as negative values. At the same time, in these compounds one of the hydrogens in the same *tert*-butyl group is involved in a weak hydrogen bond with the Cl ligand (H···Cl 2.65–2.72 Å). The latter hydrogen undergoes a down-field shift (2.83, 3.55 and 3.71 ppm in **2a**, **2c** and **2e**, respectively) that fully counterbalances the up-field shift of the agostic hydrogen, such that the overall changes in δ(^{t}Bu) are very minor.

Electrochemical study

To gain further insight we performed an electrochemical study of **2a**, **2a-COOCF$_3$**, **1a**, **1a-COOCF$_3$**, as well as **1b′** (X = MeOOC–), **1c**, and **1g** (X = OMe) (Table 2). THF and, in a few experiments, DCM were used as solvents, glassy carbon was taken as a working electrode, and the Ag/Ag$^+$ redox system was used as the reference electrode. Potentials are reported *versus* the Fc/Fc$^+$ couple. Notably, considerable complications presumably related to the adsorption on the electrode were noted. To obtain reproducible cyclic voltammograms (CVs), the application of a negative potential at the end was required (see Fig. S5† for more details).

Table 1 A(na)gostic bonds in **2**-type compounds

Complex	**2a-COOCF$_3$**	**2a**	**2c**	**2e**[a]
Ir–H calc. (exp.), Å	2.56 (2.49)	2.48	2.39	2.40 (2.34)
Ir–C, calc. (exp.), Å	3.17 (3.16)	3.13	3.07	3.08 (3.02)
δ(Ir···H), calc.	0.75	−0.60	−1.00	−0.87
δ(^{t}Bu), calc.	1.13	1.15	1.16	1.18
δ(^{t}Bu), exp.	1.16	1.20	1.11	1.11

[a] Experimental data for complex **2e** is taken from ref. 22.

Table 2 Summary of electrochemical data for the oxidation of iridium pincer complexes in THF

Complex	X =	E_p^{ox}, V	E_p^{red}, V	$E^{1/2}$	$E_{calc}^{1/2}$
2a	H	0.664	0.479	0.572	0.307
2a-COOCF$_3$	H	0.799	0.649	0.724	0.319
1a	H	0.721	—	—	0.328
1a-COOCF$_3$	H	0.902	—	—	0.367
1b′	MeOOC	1.080[a]	—	—	0.459
1g	MeO	0.395; 0.520	0.334		−0.001
1c	H	0.476	—	—	0.167

[a] Two-electron wave.

Compound **2a** revealed a partially reversible oxidation wave at E_p^{ox} = 0.664 V ($E^{1/2}$ = 0.572 V; Fig. 2). The ΔE_p and i_p values, when compared to those of the ferrocene couple, argued for a one-electron oxidation. Judging from the scan rate dependence of i_p^{red}/i_p^{ox} (increases upon increasing the scan rate), oxidation is possibly coupled to a chemical reaction that gives electrochemically inactive products. Also, an irreversible reduction wave was observed at E_p^{red} = −2.556 V that corresponds to placing an electron on the LUMO. At high scan rates some unidentified electrochemically active products of the reduction were noted. A similar pattern was observed for **2a-COOCF$_3$**, with E_p^{ox} shifted to a more positive potential.

The oxidation of **1a** revealed an irreversible wave at E_p^{ox} = 0.721 V. If the potential range is extended, two smaller, overlapping oxidation waves are observed at *ca.* 1.05 and 1.15 V, as well as a reduction shoulder-like wave at *ca.* 0.90 V (Fig. 3). We have also briefly examined the analogues of **1a** with X = MeOOC-(**1b′**) and MeO-(**1g**) (Table 2). Complex **1b′** revealed an oxidation wave shifted to a more positive potential compared to that of **1a**, while for **1g** two nearly coinciding oxidation waves were observed, and one reduction wave, that is close, but does not match precisely the reduction wave observed for **2g** (Fig. S3†). Complex **1c** revealed an irreversible oxidation wave at E_p^{ox} = 0.476 V.

DFT calculated one-electron oxidation potentials are in a reasonable agreement with the experimental data (Table 2).

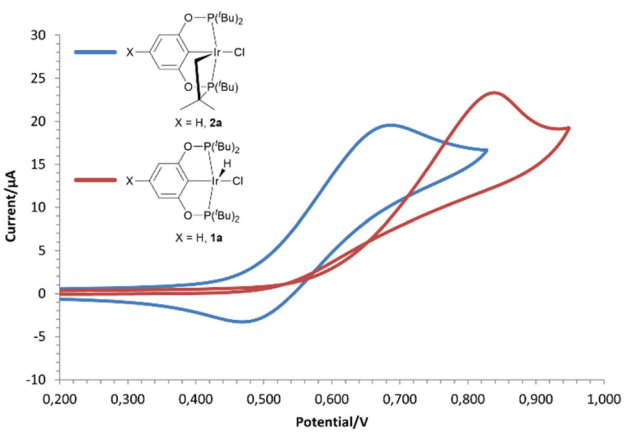

Fig. 2 Cyclic voltammograms of **1a** and **2a** in THF, scan rate 0.05 V s^{-1}.

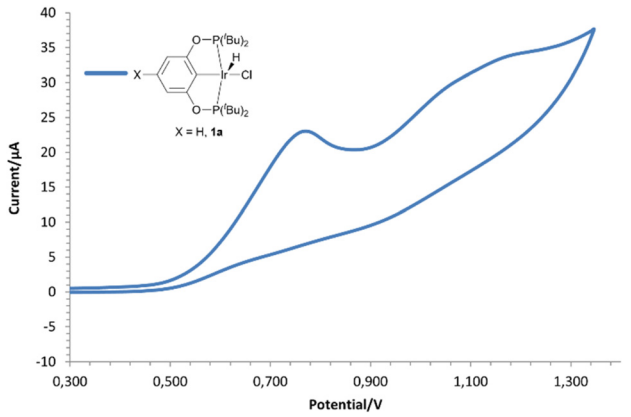

Fig. 3 Cyclic voltammogram of **1a** in THF, scan rate 0.05 V s^{-1}, extended range of potentials.

One could note a systematic shift of *ca.* 0.3 V between the experimental and calculated $E^{1/2}$ values; presumably, this could be due to inaccuracies in the continuum solvation model.[24]

To sum up, most of the type **1** compounds undergo a one-electron oxidation with the formation of Ir(IV) species $\mathbf{1}^{\bullet+}$; the latter undergoes subsequent transformations presumably associated with the hydride ligand, as suggested by comparison with the electrochemically more stable type **2** compounds. No unambiguous evidence that **2** is formed upon electrochemical oxidation of **1** was obtained.

Previously, Speiser *et al.* reported[25] two reduction waves for **1c**, one of which was interpreted as the formation of **2c** through a so-called "square scheme" mechanism. A straightforward comparison with our results is not possible due to the different conditions used. We note, though, that an as-proposed direct conversion of $\mathbf{1c}^{\bullet+}$ to $\mathbf{2c}^{\bullet+}$ with the evolution of hydrogen is not possible for thermodynamic reasons (unless an effective purging was used); thus, the calculated ΔG for **1c** = **2c** + H_2 is +17.5 kcal mol^{-1}, and +12.9 kcal mol^{-1} for $\mathbf{1c}^{\bullet+}$ = $\mathbf{2c}^{\bullet+}$ + H_2. If $\mathbf{2c}^{\bullet+}$ was indeed formed, it was most likely through disproportionation reactions, for example the reaction 2 × (PCP)$IrHCl^{\bullet+}$ ($\mathbf{1c}^{\bullet+}$) = (PCP)Ir^+ + (PCP)$Ir^{\bullet}$ + H_2 has a more favourable ΔG = −33.8 kcal mol^{-1}. (PCP)Ir^+, as will be shown below, can further convert to $\mathbf{2c}^+$.

Mechanism of conversion of 1 to 2

The known cyclometallations of an internal *tert*-butyl group in iridium pincer complexes proceed very slowly or under harsh conditions. Some examples include deuterium scrambling between *tert*-butyls and hydridic positions in (*p*-H-POCOP)IrH_2 (slow at rt, with complete deuteration upon prolonged heating at 120 °C and above),[26] dehydrogenative metallation of the *tert*-butyl group in (PCyP)IrH_2 at 120 C° and at 200 °C in (PCyP)IrHCl,[27] metallation of the *p*-MeO–PCP pincer ligand at 80 °C for 24 h, that gives a mixture of (*p*-MeO–PCP)IrHCl and a complex with metallated *tert*-butyl group **2e**.[22] Mechanistic studies[27] suggested oxidative addition of the C–H bond to Ir(III) IrH_2 or IrHCl centres to give Ir(V) as a plausible pathway.

Given the mild conditions of the **1** to **2** conversion reported here, it is likely that another mechanism of C–H activation is involved. It is logical to propose that the reaction begins with oxidation of **1a** to give $\mathbf{1a}^{\bullet+}$. Then, an oxidant anion can abstract H^+ from $\mathbf{1a}^{\bullet+}$ with the formation of Ir(II) complex $\mathbf{i}^{\bullet}$ (Scheme 4). From that point, there are two possible pathways. One option is that $\mathbf{i}^{\bullet}$ can undergo oxidation to the Ir(III) complex **ii**, from which a low-energy **1a-TS1** (15.9 kcal mol^{-1}) leads to a product with a cyclometallated *tert*-butyl group, **iii** (Scheme 4, red). Subsequently, abstraction of H^+ from **iii** or the energetically close **iv** with an oxidant anion leads to the product **2a**. The same mechanism is energetically viable for the **1c** to **2c** conversion as well, with **1c-TS1** and **1c-iii** located at +2.4 and −6.7 kcal mol^{-1} *versus* **1c-ii**. This mechanism may be relevant to the above-mentioned reaction of **1a** with acids as well, with **ii** being generated through the protonation of hydrides or H^+ serving as an oxidant. Alternatively, $\mathbf{i}^{\bullet}$ can undergo C–H activation directly through **1a-TS3** to give complex **v** (Scheme 4, blue). Oxidation of **v** would then lead to

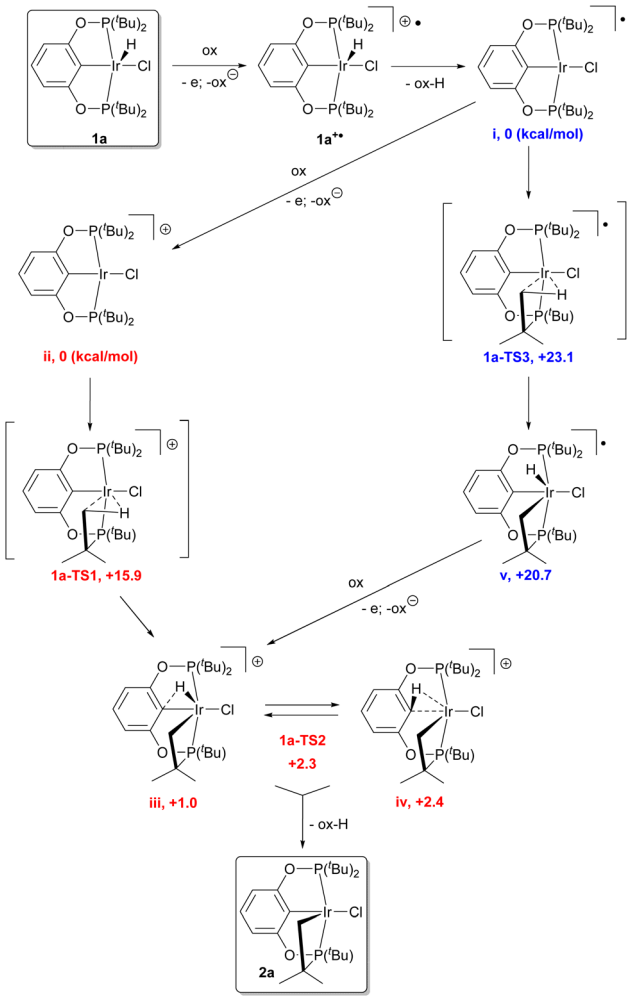

Scheme 4 Possible mechanism for the oxidation-induced C–H bond activation in iridium pincer complexes. "Ox" denotes oxidant. DFT calculated Gibbs free energies are given in kcal mol^{-1} *versus* complexes **i** and **ii**.

iii. We slightly favour the pathway through **ii** and **1a-TS1**, because we expect **i** to be oxidized readily ($E^{1/2}_{calc}$ = 0.079 V); however more studies are needed to make a reliable choice.

If the proposed mechanism is correct, one could envision the possibility that 14e cationic complexes similar to **ii** mediate oxidation-driven C–H activations and dehydrogenations in a manner similar to the mediation of 14e (pincer)Ir species in the dehydrogenation of alkanes. Scheme 5 depicts a comparison of the hypothetical catalytic cycle of ethane dehydrogenation through (^{Me4}POCOP)IrCl$^+$ (that employs two equivalents of oxidant and base as a driving force) with the traditional catalytic cycle through (^{Me4}POCOP)Ir (that employs a sacrificial hydrogen acceptor as the driving force). A ligand with methyl groups replacing *tert*-butyls was taken as a model. From the electronic point of view, it can be seen that the key transition states for both pathways are energetically accessible; the slowest steps are β-elimination for the (^{Me4}POCOP)IrCl$^+$ cycle (+23.2 kcal mol^{-1}) and ethylene dissociation for the (^{Me4}POCOP)Ir cycle (+16.0 kcal mol^{-1}). To enable the cycle through (pincer)IrCl$^+$, possibly pincer ligands that are more reluctant to intramolecular C–H activation would be required, for example, fluorinated ligands.[28] Also, important is that H$^+$ would be effectively removed from the oxidized species, while the hydride in the parent IrHCl compound would remain unaffected.

Recently, a conceptually similar dehydrogenation was reported. Thus, Goldman and Miller[15] generated (pincer)Ir from (PCP)IrH$_2$ and (POCOP)IrH$_2$ using two equivalents of oxidant and base, through two consecutive proton removals. The (pincer)Ir species were then reacted with alkanes to give alkenes, with recovery of (pincer)IrH$_2$. While perhaps being a step towards something bigger, the reported process uses the traditional pathway through electron-rich (pincer)Ir and (pincer)IrH$_2$, and thus is sensitive to over-oxidation.[15] Hence, more electron-deficient species are desired to enable the use of cheap and powerful oxidants, such as oxygen. It could be that the pathway through (pincer)IrCl$^+$ could offer some alternatives in that respect. For example, **1a** is reasonably air-stable, and oxidation with CF_3COOAg to give **2a** can be performed in air.

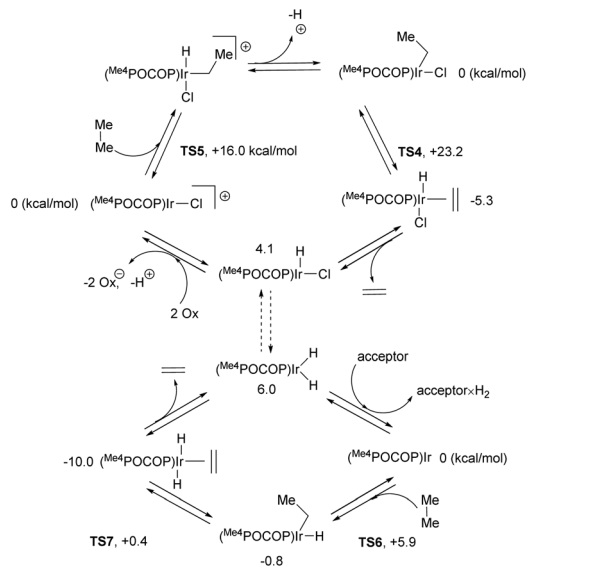

Scheme 5 DFT modelled comparison of the dehydrogenation of ethane through 14e (^{Me4}POCOP)IrCl$^+$ that can be driven by oxidation (top), with the traditional dehydrogenation through 14e (^{Me4}POCOP)Ir that is driven by a sacrificial hydrogen acceptor (bottom).

Conclusions

To sum up, we have reported oxidations of iridium pincer complexes **1a** and **1c** with CF_3COOAg and [FcAc]PF$_6$, respectively, to give compounds **2a-COOCF$_3$** and **2c** with cyclometallated *tert*-butyl groups. This transformation thus represents oxidation-induced C–H activation. An electrochemical study and DFT calculations provided a mechanistic guess that involves (pincer)IrCl$^+$ (or –COOCF$_3$) as the compound responsible for C–H activation. Interestingly, some analogies could be drawn between the reactivity of (pincer)IrCl$^+$ and (pincer)Ir, with the latter being a key compound in the catalytic cycle for alkane dehydrogenation. Thus, (pincer)IrCl$^+$ or related species hold some promise to substitute (pincer)Ir in oxidation-driven dehydrogenation reactions, since the electron-poor (pincer)IrCl$^+$ species are expected to be more stable with respect to undesired over-oxidation.

Experimental part

General considerations

All the manipulations were conducted under an argon atmosphere using standard Schlenk techniques unless otherwise stated. All the solvents (including deuterated) were distilled under an argon atmosphere from the appropriate drying agents. Commercially available reagents were used as received. Compounds **1a**,[26] **1b′**,[29] **1c**,[30] and **1g**[26] were prepared according to literature procedures. NMR spectra were recorded on Bruker Avance 400 MHz and Bruker Avance 500 MHz spectrometers. ^{1}H NMR chemical shifts are reported in parts per million downfield from tetramethylsilane; the residual signals of the deuterated solvent were used as a reference. ^{31}P{^{1}H} NMR chemical shifts are reported relative to an external 85% solution of phosphoric acid in D$_2$O. ^{19}F{^{1}H} NMR chemical shifts are reported relative to external CFCl$_3$. Elemental analyses were performed at the A. N. Nesmeyanov Institute of Organoelement Compounds of RAS.

Reaction of complex 1a with one equivalent of CF_3COOAg. Formation of complex 1-COOCF$_3$

To a solution of complex **1a** (0.063 g, 0.101 mmol) in THF (15 ml) in a light-protected flask a solution of CF_3COOAg (0.023 g, 0.104 mmol) in THF (5 ml) was added dropwise. This was accommodated by a colour change from red-orange to yellow-orange and the formation of a precipitate. The reaction

mixture was stirred for an additional 2.5 hours, the volatiles were removed in vacuum and the residue was extracted with CH_2Cl_2 and filtered through a thin layer of Celite™. After evaporation of the volatiles and drying in a vacuum, complex **1-COOCF$_3$** (0.069 g, 97%) was obtained as a yellow-orange powder. Calculated for $C_{24}H_{40}F_3IrO_4P_2$: C, 40.96; H, 5.73. Found: 41.17; H, 5.64. ^{1}H NMR (400 MHz, $CDCl_3$): δ 6.73 (t, 1H, $^3J_{HH}$ = 8.0 Hz, Ar–H), 6.48 (d, 2H, $^3J_{HH}$ = 8.0 Hz, Ar–H), 1.36–1.31 (m, 36 H, 4 C(CH$_3$)$_3$), −38.98 (t, 1H, $^3J_{PH}$ = 12.7 Hz). ^{31}P{^{1}H} NMR (1612 MHz, $CDCl_3$): δ 172.0 (s). ^{19}F{^{1}H} NMR (377 MHz, $CDCl_3$): δ −75.0 (s). ^{13}C NMR (126 MHz, C_6D_6) δ 167.14 (vt, J = 5.9 Hz, 2-C and 6-C), 164.90 (q, $^2J_{C–F}$ = 37.4 Hz, *C*O–CF$_3$), 125.92 (s, 4-C), 118.06 (q, $^2J_{C–F}$ = 287 Hz, CO–*C*F$_3$) 108.86 (m, 1-C), 105.22 (vt, J = 5.3 Hz, 3-C and 5-C), 42.76 (vt, J = 12.1 Hz, *C*(CH$_3$)$_3$), 39.83 (vt, J = 12.4 Hz, *C*(CH$_3$)$_3$), 27.78 (vt, J = 3.2 Hz, C(*C*H$_3$)$_3$), 27.30 (vt, J = 3.0 Hz, C(*C*H$_3$)$_3$).

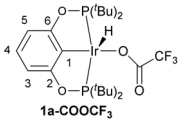

1a-COOCF$_3$

Reaction of complex 1a with an excess of CF$_3$COOAg. Formation of complex 2a

To a solution of complex **1a** (0.046 g, 0.074 mmol) in THF (15 ml) in a light-protected flask a solution of CF_3COOAg (0.066 g, 0.299 mmol) in THF (5 ml), was added dropwise. This was accommodated by a colour change from red-orange to yellow-orange and the formation of a precipitate. The reaction mixture was stirred for an additional 30 min, the volatiles were removed in a vacuum and the residue was extracted several times with pentane and filtered through a thin layer of Celite™. After evaporation of the volatiles and drying in a vacuum complex, **2a** (0.047 g, 90%) was obtained as a yellow-orange powder. Calculated for $C_{24}H_{38}F_3IrO_4P_2$: C, 41.08; H, 5.46. Found: C, 40.89; H, 5.47. ^{1}H NMR (400 MHz, $CDCl_3$): δ 6.84 (apparent t, 1H, J = 8.0 Hz, Ar–H), 6.67 (d, 2H, $^3J_{HH}$ = 8.0 Hz, Ar–H), 6.64 (d, 2H, $^3J_{HH}$ = 8.0 Hz, Ar–H), 2.79 (ddd, 1H, J_1 = 9.7 Hz, J_2 = 6.0 Hz, J_3 = 1.6 Hz, Ir–C*H*$_2$), 2.08–2.05 (m, 1H, Ir–C*H*$_2$), 1.42 (d, 9H, $^3J_{PH}$ = 15.7 Hz, –C(CH$_3$)$_3$), 1.42 (overlapping d, 3H, $^3J_{PH}$ ≈ 15.7 Hz, Ir–CH$_2$–C(C*H*$_3$)$_2$), 1.24 (d, 9H, $^3J_{PH}$ = 14.7 Hz, –C(CH$_3$)$_3$), 1.16 (d, 9H, –C(CH$_3$)$_3$), $^3J_{PH}$ = 14.1 Hz, 0.95 (d, 3H, $^3J_{PH}$ = 12.4 Hz, Ir–CH$_2$–C(C*H*$_3$)$_2$). ^{31}P{^{1}H} NMR (161.98 MHz, $CDCl_3$): δ 159.1 (d, $^2J_{PP}$ = 367.4 Hz), 113.5 (d, $^2J_{PP}$ = 367.4 Hz). ^{19}F{^{1}H} NMR (376.50 MHz, $CDCl_3$): δ −74.9 (s). ^{13}C NMR (126 MHz, C_6D_6) δ 168.10 (dd, $^2J_{C–P}$ = 8.0 Hz, $^3J_{C–P}$ = 5.2 Hz, 2-C or 6-C), 165.73 (dd, $^2J_{C–P}$ = 7.2 Hz, $^3J_{C–P}$ = 3.3 Hz, 2-C or 6-C), 164.93 (q, $^2J_{C–F}$ = 36.7 Hz, CO–*C*F$_3$), 126.84 (s, 4-C), 116.74 (apparent t, $^2J_{C–P1}$ = $^2J_{C–P2}$ = 3.3 Hz, 1-C), 117.79 (q, $^2J_{C–F}$ = 288 Hz, CO–*C*F$_3$), 105.95 (d, $^3J_{C–P}$ = 11.0 Hz, 3-C or 5-C), 105.64 (d, $^3J_{C–P}$ = 11.0 Hz, 3-C or 5-C), 66.10 (dd, $^1J_{C–P}$ = 18.6 Hz, $^3J_{C–P}$ = 5.0 Hz, P–*C*(CH$_3$)$_2$–CH$_2$–), 45.09 (dd, $^1J_{C–P}$ = 17.5 Hz, $^3J_{C–P}$ = 5.4 Hz, *C*(CH$_3$)$_3$), 39.81–39.47 (m, overlapping, 2 × *C*(CH$_3$)$_3$), 27.23–27.09 (m, overlapping, 2 × C(*C*H$_3$)$_3$), 26.12 (dd, $^2J_{C–P}$ = 4.4 Hz, $^4J_{C–P}$ = 1.1 Hz, C(*C*H$_3$)$_3$), 24.08 (d, $^2J_{C–P}$ = 3.9 Hz, CH$_3$), 22.96 (d, $^2J_{C–P}$ = 4.7 Hz, CH$_3$), −3.90 (dd, $^2J_{C–P}$ = 25.4 Hz, $^2J_{C–P}$ = 2.3 Hz, –CH$_2$–Ir).

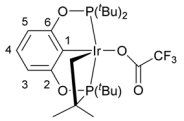

2a-COOCF$_3$

Reaction of complex 1c with acetyl–ferrocenium hexafluorophosphate. Formation of complex 2c

To a solution of complex **1c** (0.030 g, 0.048 mmol) in THF (15 ml), a solution of acetyl–ferrocenium hexafluorophosphate (0.036 g, 0.096 mmol) in THF (5 ml) was added. The reaction mixture was stirred overnight, the volatiles were removed in a vacuum and the residue was purified by flash chromatography on silica gel using a hexane–benzene mixture as the eluent. After evaporation of the volatiles, the residue was dissolved in hexane and crystallized. Complex **2c** (0.014 g, 47%) was obtained as a red solid. Calculated for $C_{24}H_{42}ClIrP_2$: C, 46.48; H, 6.83. Found: C, 46.57; H, 6.70. ^{1}H NMR (500 MHz, C_6D_6) δ 7.22–7.14 (m, overlapping, 2H, 3-C and 5-C), 7.03 (t, $^3J_{HH}$ = 7.3 Hz, 1H, 4-H), 4.36–4.26 (m, 1H, –CH$_2$–P), 3.53 (ddd, J_1 = 8.9 Hz, J_2 = 5.1 Hz, J_3 = 2.0 Hz, 1H, Ir–CH$_2$), 3.20–3.00 (m, 3H, –CH$_2$–P), 2.14–2.09 (m, 1H, Ir–CH$_2$), 1.49 (d, $^3J_{PH}$ = 13.7 Hz, 3H, Ir–CH$_2$–C(C*H*$_3$)$_2$), 1.34 (d, $^3J_{PH}$ = 13.7 Hz, 9H, –C(CH$_3$)$_3$), 1.17 (d, $^3J_{PH}$ = 12.8 Hz, 9H, –C(CH$_3$)$_3$), 1.11 (d, $^3J_{PH}$ = 12.7 Hz, 9H, –C(CH$_3$)$_3$), 0.72 (d, $^3J_{PH}$ = 12.8 Hz, 3H, Ir–CH$_2$–C(C*H*$_3$)$_2$). ^{31}P NMR (162 MHz, C_6D_6) δ 48.93 (d, $^2J_{PP}$ = 349.2 Hz), 7.85 (d, $^2J_{PP}$ = 349.2 Hz). ^{13}C NMR (126 MHz, C_6D_6) δ 152.22 (dd, $^2J_{C–P}$ = 13.7 Hz, $^3J_{C–P}$ = 5.1 Hz, 2-C or 6-C), 151.09 (s, 1-C), 149.15 (dd, $^2J_{C–P}$ = 10.4 Hz, $^3J_{C–P}$ = 4.2 Hz, 2-C or 6-C), 123.54 (apparent t, $^4J_{C–P1}$ = $^4J_{C–P2}$ = 1.2 Hz, 4-C), 122.43 (d, $^3J_{C–P}$ = 16.3 Hz, 3-C or 5-C), 121.86 (d, $^3J_{C–P}$ = 15.9 Hz, 3-C or 5-C), 59.43 (dd, $^1J_{C–P}$ = 20.4 Hz, $^3J_{C–P}$ = 2.2 Hz, P–*C*(CH$_3$)$_2$–CH$_2$–), 40.90 (dd, $^1J_{C–P}$ = 16.5 Hz, $^3J_{C–P}$ = 3.1 Hz, *C*(CH$_3$)$_3$), 36.65 (apparent t, $^1J_{C–P}$ = $^3J_{C–P}$ = 8.1 Hz, *C*(CH$_3$)$_3$), 34.97 (dd, $^1J_{C–P}$ = 14.7 Hz, $^3J_{C–P}$ = 4.8 Hz, *C*(CH$_3$)$_3$), 34.26 (dd, $^1J_{C–P}$ = 15.2 Hz, $^3J_{C–P}$ ≈ 1.2 Hz, P–CH$_2$–Ir), 34.05 (dd, $^1J_{C–P}$ = 13.9 Hz, $^3J_{C–P}$ ≈ 1.2 Hz, P–CH$_2$–Ir), 30.44 (dd, $^2J_{C–P}$ = 3.8 Hz, $^4J_{C–P}$ = 1.5 Hz, C(*C*H$_3$)$_3$), 29.17 (dd, $^2J_{C–P}$ = 2.7 Hz, $^4J_{C–P}$ = 1.7 Hz, C(*C*H$_3$)$_3$), 29.02 (dd, $^2J_{C–P}$ = 3.3 Hz, $^4J_{C–P}$ = 1.6 Hz, C(*C*H$_3$)$_3$), 27.06 (dd, $^2J_{C–P}$ = 3.9 Hz, $^4J_{C–P}$ ≈ 0.9 Hz, CH$_3$), 26.08 (s, CH$_3$), −6.00 (dd, $^2J_{C–P}$ = 23.3 Hz, $^2J_{C–P}$ = 2.3 Hz, –CH$_2$–Ir).

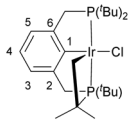

2c

X-ray crystallography

Intensity data were collected with an Oxford Diffraction Excalibur 3 system, using ω-scans and Mo Kα (λ = 0.71073 Å) radiation.[31] The data were extracted and integrated using Crysalis RED.[32] The structures were solved and refined by full-matrix least-squares calculations on F^2 using JANA2006.[33] Molecular graphics were generated using Mercury 3.10.3.[34]

Cyclic voltammetry

Cyclic voltammetry measurements were performed on an Autolab PGSTAT101 potentiostat for 10^{-3} M solutions in rigorously dried and degassed THF (or CH_2Cl_2) in a standard three-electrode cell equipped with a glassy carbon working electrode (S = 7 mm^2), platinum wire as the counter electrode, and Ag/Ag^+ as the reference electrode. NBu_4PF_6 was used as the supporting electrolyte at the 0.1 M concentration. The scan rate was 0.02–1 V s^{-1}. Ferrocene–ferrocenium (Fc/Fc^+) pair was applied as the external standard.

Computational details

DFT calculations were performed with ORCA 4.1.1,[35] using the PBE functional[36] with a D3BJ dispersion correction.[37] For geometry optimization and frequencies, the def2-SVP basis set[38] was used, while the def2-TZVPP[38] basis set was used for single-point energies. The RI algorithm with appropriate fitting basis sets was exploited. Solvent effects were incorporated using the CPCM solvation model[39] with DCM used as the solvent. Redox potentials were calculated using the $E^\circ = \Delta G(\mathrm{ox})/-nF$ expression, where ΔG is the Gibbs free energy difference between the neutral and oxidized species, F is the Faraday constant, and n is number of electrons. Some of the cation-radical species reveal very small negative frequencies; these were not given any special treatment due to the expected negligible effect on E°. Computed redox potentials were referred to the ferrocene–ferrocenium (Fc/Fc^+) pair. NMR spectra were calculated using the ZORA[40] two-component approximation to relativistic effects, with the SARC–ZORA–TZVPP[41] basis set used for Ir and the ZORA–def2–TZVPP basis set for other atoms.

Conflicts of interest

There are no conflicts to declare.

Acknowledgements

This work has received no dedicated external funding. We gratefully acknowledge Dr S. M. Peregudova for her kind assistance in the initial attempts of the electrochemical studies.

References

1 (*a*) B. A. Arndtsen, R. G. Bergman, T. A. Mobley and T. H. Peterson, *Acc. Chem. Res.*, 1995, **28**, 154–162; (*b*) K. I. Goldberg and A. S. Goldman, *Acc. Chem. Res.*, 2017, **50**, 620–626.

2 For selected reviews on pincer complexes, see: (*a*) L. Piccirilli, D. L. J. Pinheiro and M. Nielsen, *Catalysts*, 2020, **10**, 773; (*b*) H. Valdés, E. Rufino-Felipe and D. Morales-Morales, *J. Organomet. Chem.*, 2019, **898**, 120864; (*c*) M. A. W. Lawrence, K.-A. Green, P. N. Nelson and S. C. Lorraine, *Polyhedron*, 2018, **143**, 11–27; (*d*) H. Valdés, M. A. García-Eleno, D. Canseco-Gonzalez and D. Morales-Morales, *ChemCatChem*, 2018, **10**, 3136–3172; (*e*) E. Peris and R. H. Crabtree, *Chem. Soc. Rev.*, 2018, **47**, 1959–1968; (*f*) *Pincer Compounds: Chemistry and Applications*, ed. D. Morales-Morales, Elsevier, The Netherlands, 2018; (*g*) H. Valdés, L. González-Sebastián and D. Morales-Morales, *J. Organomet. Chem.*, 2017, **845**, 229–257; (*h*) M. Asay and D. Morales-Morales, *Dalton Trans.*, 2015, **44**, 17432–17447; (*i*) *The Chemistry of Pincer Compounds*, ed. D. Morales-Morales and C. Jensen, Elsevier, The Netherlands, 2007.

3 For dehydrogenation by iridium pincer complexes, see: (*a*) J. Choi, A. H. R. MacArthur, M. Brookhart and A. S. Goldman, *Chem. Rev.*, 2011, **111**, 1761–1779; (*b*) A. Kumar, T. M. Bhatti and A. S. Goldman, *Chem. Rev.*, 2017, **117**, 12357–12384; (*c*) A. V. Polukeev and O. F. Wendt, *J. Organomet. Chem.*, 2018, **867**, 33–50; (*d*) D. Morales-Morales, R. Redón, C. Yung and C. M. Jensen, *Inorg. Chim. Acta*, 2004, **357**, 2953–2956; (*e*) C. M. Jensen, *Chem. Commun.*, 1999, 2443–2449; (*f*) F. Liu, E. B. Pak, B. Singh, C. M. Jensen and A. S. Goldman, *J. Am. Chem. Soc.*, 1999, **121**, 4086–4087.

4 T. Tian, Z. Li and C.-J. Li, *Green Chem.*, 2021, **23**, 6789–6862.

5 For selected reviews, see: (*a*) A. E. Shilov and G. B. Shul'pin, *Chem. Rev.*, 1997, **97**, 2879–2932; (*b*) J. A. Labinger, *Chem. Rev.*, 2017, **117**, 8483–8496; (*c*) N. J. Gunsalus, A. Koppaka, S. H. Park, S. M. Bischof, B. G. Hashiguchi and R. A. Periana, *Chem. Rev.*, 2017, **117**, 8521–8573.

6 N. Sauermann, T. H. Meyer, Y. Qiu and L. Ackermann, *ACS Catal.*, 2018, **8**, 7086–7103.

7 See, for example: (*a*) M. C. Lehman, D. R. Pahls, J. M. Meredith, R. D. Sommer, D. M. Heinekey, T. R. Cundari and E. A. Ison, *J. Am. Chem. Soc.*, 2015, **137**, 3574–3584; (*b*) A. J. Ingram, A. B. Wolk, C. Flender, J. Zhang, C. J. Johnson, U. Hintermair, R. H. Crabtree, M. A. Johnson and R. N. Zare, *Inorg. Chem.*, 2014, **53**, 423–433; (*c*) M. Zhou, D. Balcells, A. R. Parent, R. H. Crabtree and O. Eisenstein, *ACS Catal.*, 2012, **2**, 208–218; (*d*) E. V. Sackville, G. Kociok-Köhn and U. Hintermair, *Organometallics*, 2017, **36**, 3578–3588; (*e*) M. C. Lehman, P. D. Boyle, R. D. Sommer and E. A. Ison, *Organometallics*, 2014, **33**, 5081–5084; (*f*) S. K. Gupta and J. Choudhury, *Dalton Trans.*, 2015, **44**, 1233–1239; (*g*) S. Hohloch, S. Kaiser, F. L. Duecker, A. Bolje, R. Maity, J. Košmrljb and B. Sarkar, *Dalton Trans.*, 2015, **44**, 686–693; (*h*) M. E. Kerr, I. Ahmed, A. Gunay, N. J. Venditto, F. Zhu, E. A. Ison and M. H. Emmert, *Dalton Trans.*, 2016, **45**, 9942–9947; (*i*) Y. Yan, Y. Chen, M. Yan, X. Li and W. Zeng, *Catal. Commun.*, 2013, **35**, 64–67; (*j*) M. Zhou, U. Hintermair, B. G. Hashiguchi, A. R. Parent, S. M. Hashmi, M. Elimelech, R. A. Periana, G. W. Brudvig and R. H. Crabtree, *Organometallics*, 2013, **32**, 957–965; (*k*) M. Zhou, N. D. Schley and R. H. Crabtree, *J. Am. Chem. Soc.*, 2010, **132**, 12550–12551.

8 J.-I. Ito, T. Kaneda and H. Nishiyama, *Organometallics*, 2012, **31**, 4442–4449.
9 K. E. Allen, D. M. Heinekey, A. S. Goldman and K. I. Goldberg, *Organometallics*, 2013, **32**, 1579–1582.
10 D. R. Pahls, K. E. Allen, K. I. Goldberg and T. R. Cundari, *Organometallics*, 2014, **33**, 6413–6419.
11 K. E. Allen, D. M. Heinekey, A. S. Goldman and K. I. Goldberg, *Organometallics*, 2014, **33**, 1337–1340.
12 M. Zhou, S. I. Johnson, Y. Gao, T. J. Emge, R. J. Nielsen, W. A. Goddard III and A. S. Goldman, *Organometallics*, 2015, **34**, 2879–2888.
13 A. G. Walden, A. Kumar, N. Lease, A. S. Goldman and A. J. M. Miller, *Dalton Trans.*, 2016, **45**, 9766–9769.
14 B. M. Lindley, A. G. Walden, A. M. Brasacchio, A. Casuras, N. Lease, C.-H. Chen, A. S. Goldman and A. J. M. Miller, *Chem. Sci.*, 2019, **10**, 9326–9330.
15 A. D. R. Shada, A. J. M. Miller, T. J. Emge and A. S. Goldman, *ACS Catal.*, 2021, **11**, 3009–3016.
16 A. V. Polukeev, S. A. Kuklin, P. V. Petrovskii, F. M. Dolgushin, M. G. Ezernitskaya and A. A. Koridze, *Russ. Chem. Bull., Int. Ed.*, 2010, **59**, 745–749.
17 A. V. Polukeev, PhD Thesis, A. N. Nesmeyanov Institute of Organoelement Compounds, RAS, 2012.
18 For heterobimetallic pincer complexes, see: (*a*) H. Valdés, J. M. Germán-Acacio, G. van Koten and D. Morales-Morales, *Dalton Trans.*, 2022, **51**, 1724–1744; (*b*) N. Á. Espinosa-Jalapa, S. Hernández-Ortega, D. Morales-Morales and R. Le Lagadec, *J. Organomet. Chem.*, 2012, **716**, 103–109; (*c*) S. A. Kuklin, A. M. Sheloumov, F. M. Dolgushin, M. G. Ezernitskaya, A. S. Peregudov, P. V. Petrovskii and A. A. Koridze, *Organometallics*, 2006, **25**, 5466–5476.
19 M. Rimoldi, A. Nakamura, N. A. Vermeulen, J. J. Henkelis, A. K. Blackburn, J. T. Hupp, J. F. Stoddart and O. K. Farha, *Chem. Sci.*, 2016, **7**, 4980–4984.
20 M. Brookhart, M. L. H. Green and G. Parkin, *Proc. Natl. Acad. Sci. U. S. A.*, 2007, **104**, 6908–6914.
21 Y. Garcıa-Rodeja, F. Feixas, E. Matito and M. Sola, *Phys. Chem. Chem. Phys.*, 2022, **24**, 29333–29337.
22 H. A. Y. Mohammad, J. C. Grimm, K. Eichele, H.-G. Mack, B. Speiser, F. Novak, M. G. Quintanilla, W. C. Kaska and H. A. Mayer, *Organometallics*, 2002, **21**, 5775–5784.
23 A. Arunachalampillai, D. Olsson and O. F. Wendt, *Dalton Trans.*, 2009, 8626–8630.
24 M. Isegawa, F. Neese and D. A. Pantazis, *J. Chem. Theory Comput.*, 2016, **12**, 2272–2284.
25 F. Novak, B. Speiser, H. A. Y. Mohammad and H. A. Mayer, *Electrochim. Acta*, 2004, **49**, 3841–3853.
26 I. Gottker-Schnetmann and M. Brookhart, *J. Am. Chem. Soc.*, 2004, **126**, 9330–9338.
27 A. V. Polukeev, R. Marcos, M. S. G. Ahlquist and O. F. Wendt, *Chem. Sci.*, 2015, **6**, 2060–2067.
28 B. C. Gruver, J. J. Adams, S. J. Warner, N. Arulsamy and D. M. Roddick, *Organometallics*, 2011, **30**, 5133–5140.
29 N. T. Mucha and R. Waterman, *Organometallics*, 2015, **34**, 3865–3872.
30 C. J. Moulton and B. L. Shaw, *J. Chem. Soc., Dalton Trans.*, 1976, 1020–1024.
31 *Crysalis CCD*, Oxford Diffraction Ltd., Abingdon, Oxfordshire, UK, 2005.
32 *Crysalis RED*, Oxford Diffraction Ltd., Abingdon, Oxfordshire, UK, 2005.
33 V. Petříček, M. Dušek and L. Palatinus, Crystallographic Computing System JANA2006: General features, *Z. Kristallogr.*, 2014, **229**, 345–352.
34 C. F. Macrae, P. R. Edgington, P. McCabe, E. Pidcock, G. P. Shields, R. Taylor, M. Towler and J. van de Streek, *J. Appl. Crystallogr.*, 2006, **39**, 453–457.
35 (*a*) F. Neese, *Mol. Sci.*, 2012, **2**, 73–78; (*b*) F. Neese, *Wiley Interdiscip. Rev.: Comput. Mol. Sci.*, 2017, **8**, e1327.
36 J. P. Perdew, K. Burke and M. Ernzerhof, *Phys. Rev. Lett.*, 1996, **77**, 3865.
37 (*a*) S. Grimme, S. Ehrlich and L. Goerigk, *J. Comput. Chem.*, 2011, **32**, 1456–1465; (*b*) S. Grimme, J. Antony, S. Ehrlich and H. Krieg, *J. Chem. Phys.*, 2010, **132**, 154104.
38 F. Weigend and R. Ahlrichs, *Phys. Chem. Chem. Phys.*, 2005, **7**, 3297.
39 M. Cossi and V. Barone, *J. Phys. Chem. A*, 1998, **102**, 1995–2001.
40 R. Bouten, E. J. Baerends, E. van Lenthe, L. Visscher, G. Schreckenbach and T. Ziegler, *J. Phys. Chem. A*, 2000, **104**, 5600–5611.
41 D. A. Pantazis, X.-Y. Chen, C. R. Landis and F. Neese, *J. Chem. Theory Comput.*, 2008, **4**, 908–919.